Check for updates

Performance evaluation of photolytic and electrochemical oxidation processes for enhanced degradation of food dyes laden wastewater

Seema Sartaj, Nisar Ali, Adnan Khan, Sumeet Malik, Muhammad Bilal, Menhad Khan, Nauman Ali, Sajjad Hussain, Hammad Khan and Sabir Khan

ABSTRACT

Wastewater containing dyes is considered as the top-priority pollutant when discharged into the environment. Herein, we report for the applicability of 254 nm ultraviolet light and electrochemical process using a titanium ruthenium oxide anode for the degradation of Allura red and erythrosine dyes. During the photolytic process, 95% of Allura red dye (50 ppm) was removed after 1 h at pH 12 and 35 °C, whereas 90% color removal of erythrosine dye (50 ppm) was achieved after 6 h of treatment at pH 6.0 and 30 °C. On the other hand, 99.60% of Allura red dye (200 ppm) was removed within 5 min by the electrochemical process applying a current density (5 mA cm^{-2}) at pH 5.0 and 0.1 mol L^{-1} sodium chloride (NaCl) electrolytic medium. Similarly, 99.61% of erythrosine dye (50 ppm) degradation was achieved after 10 min at a current density of 8 mA cm^{-2}, pH 6.0, and 0.1 mol L^{-1} of NaCl electrolyte. The minimum energy consumption value for Allura red and erythrosine dyes (0.196 and 0.941 kWh m^{-3}, respectively) was calculated at optimum current densities of 5 and 8 mA cm^{-2}. The results demonstrated that the electrochemical process is more efficient at removing dyes in a shorter time than the photolytic process since it generates powerful oxidants like the chlorine molecule, hypochlorous acid, and hypochlorite on the surface of the anode and initiates a chain reaction to oxidize the dyes molecules.

Key words | Allura red, electrochemical degradation, environmental pollution, erythrosine, optimization, photolysis

HIGHLIGHTS

- Wastewater containing toxic dye pollutants as the top-priority environmental concern.
- Photocatalytic and electrochemical methods were inspected for Allura red and erythrosine dyes degradation.
- Critical parameters affecting these processes were standardized for maximum discoloration efficiency.
- Electrochemical process triggered Allura red and erythrosine dyes removal within 5 and 10 min.
- Electrochemical oxidation as a highly efficient and promising approach for dye-harboring wastewater remediation.

Seema Sartaj
Nisar Ali
Key Laboratory for Palygorskite Science and Applied Technology of Jiangsu Province, National & Local Joint Engineering Research Center for Deep Utilization Technology of Rock-salt Resource, Faculty of Chemical Engineering,
Huaiyin Institute of Technology,
Huaian 223003, China

Seema Sartaj
Adnan Khan
Sumeet Malik
Menhad Khan
Nauman Ali
Institute of Chemical Sciences,
University of Peshawar,
Khyber Pakhtunkhwa 25120, Pakistan

Muhammad Bilal (corresponding author)
School of Life Science and Food Engineering,
Huaiyin Institute of Technology,
Huaian 223003, China
E-mail: *bilaluaf@hotmail.com*

Sajjad Hussain
Hammad Khan
Faculty of Materials & Chemical Engineering GIK,
Institute of Engineering Sciences & Technology,
23460 Topi, KP, Pakistan

Sabir Khan
Department of Analytical Chemistry, Institute of Chemistry,
State University of São Paulo (UNESP),
14801-970 Araraquara, SP, Brazil

doi: 10.2166/wst.2020.182

Downloaded from http://iwaponline.com/wst/article-pdf/81/5/971/768038/wst081050971.pdf
by guest

INTRODUCTION

Today, the entire world faces outrageous issues of safe drinking and sterile water for the consumption of human beings because of groundwater adulteration and industrial effluents (Rasheed *et al.* 2017; Gnanasekaran *et al.* 2019; Liu *et al.* 2019; Shetti *et al.* 2019). The wastewater originating from such industries contains suspended solids, organic matter, and an immense amount of dyes that have an undesirable impact on living life forms (Ali *et al.* 2018; Jager *et al.* 2018; Tiwari & Ram 2019). The presence of a little concentration of dyes in wastewater can influence the light levels in photosynthesis in amphibian plants (Ali *et al.* 2019; Bilal *et al.* 2018a, 2018b, 2018c; Salazar *et al.* 2018). The strong color of dyes is due to the azo bond and chromophore groups, which are stable to environmental factors (Veisi *et al.* 2019; Zukawa *et al.* 2019; Ali *et al.* 2020).

Among the synthetic dyes, Allura red is a dim red water-soluble food dye (Figure 1(a)), which is generally used in foodstuffs such as sweetmeats, cereals, soda pops, and bread shop items (Al-Shabib *et al.* 2019). In spite of its wide applications, its harmful effect cannot be overlooked because it contains an azo bond and may cause asthma, hypersensitivity, and hyperactivity in kids (Ostovan *et al.* 2018). Its use is prohibited in countries like Germany, Denmark, Switzerland, and Sweden (Asfaram *et al.*, 2018). Erythrosine is cherry-pink and is a water-soluble food dye (Figure 1(b)) mainly found in different food items, pharmaceutical, makeup, and textile industries. Its excessive use leads to various kinds of medical issues, including sickliness, thyroid harmfulness, sensitivities, and neurotoxicity in animals and humans (Zinatloo-Ajabshir *et al.* 2019). It is banned in the USA and Norway because of its lethal nature. The release of these toxic dyes to the environment causes an unfavorable impact on living life forms (Mazloom *et al.* 2018; Khan *et al.* 2019a, 2019b). Therefore, quick and judicious strategies are necessary for the elimination of these dyes (Khan *et al.* 2018; Zaouak *et al.* 2019).

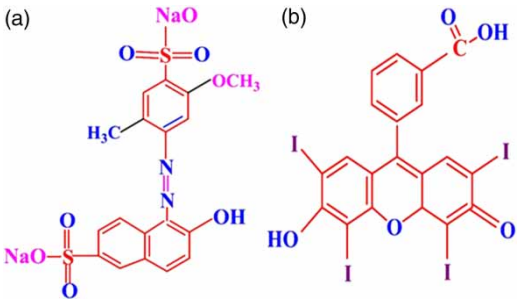

Figure 1 | Molecular structure of (a) Allura red and (b) erythrosine dye.

Various conventional biological (Martínez-Huitle & Panizza 2018) and chemical (Safni *et al.* 2019) techniques have been attempted for the treatment of wastewaters containing dye pollutants, but their outcomes are limited (Rasheed *et al.* 2018a, 2018b; Sahu *et al.* 2018). Recently, different photolytic and electrochemical-based degradation processes have been undertaken to degrade toxic food dyes because of their high efficiency, less demanding activity, eco-friendliness, flexibility, and minimal effort adequacy. In photolysis, the photochemical reactions cause the degradation of residual dyes, released into the water by transforming them into simpler compounds. The energy provided by the UV light to break bonds (Bendjama *et al.* 2019; Shi *et al.* 2018). However, photolysis necessitates a longer time duration that may result in incomplete degradation and sometimes produces intermediates that are more toxic (Zhou *et al.* 2009; Aziz *et al.* 2020). Electrochemical degradation is another advanced technique for the degradation of dyes, which involves electro-oxidation with active chlorine (a major oxidizing agent). In this case, the electro-generated free chlorine produces species like hypochlorous acid (HClO) and hypochlorite (ClO^-) oxidize the organic matter within the effluents through reactions (Equations (1)–(3)) (Nakamura *et al.* 2019).

$$2Cl^- \rightarrow Cl_2 + 2e^- \quad (1)$$

$$Cl_{2(aq)} + H_2O \rightarrow HClO^- + Cl^- + H^+ \quad (2)$$

$$\text{Dye} + ClO^- \rightarrow \text{dye intermediates} \rightarrow CO_2 + H_2O + Cl^- \quad (3)$$

For electrochemical degradation of dyes, diverse anode materials like platinum cathode, boron-doped diamond (BDD), and titanium-based dimensional stable anode (DSA) terminals have been utilized (Vasconcelos *et al.* 2019). Owing to its great chemical stability, high rates of removal in the presence of Cl^- ions, minimal effort, and environmental compatibility, titanium ruthenium oxide electrodes were applied in this work for Allura red and erythrosine dye degradation. Both the photolytic and electrochemical degradation methods were compared for erythrosine and Allura red dyes. In addition, the effect of various critical factors such as pH, current density, and the concentration of electrolyte was also studied.

MATERIALS AND METHODS

Reagents and equipment

The reagents and chemicals utilized during the trial were of scientific standard. Erythrosine (Red No. 3) and Allura

Downloaded from http://iwaponline.com/wst/article-pdf/81/5/971/768038/wst081050971.pdf
by guest

(Red No. 40) dyes were acquired from Sigma Aldrich, USA. Sodium chloride (NaCl), sodium sulfate (Na_2SO_4), and sodium nitrate ($NaNO_3$) were obtained from Merck, Germany. All the necessary solutions were prepared using deionized water. The equipment used was DAZHENG DC Power Supply (model-PS-303D), double-beam UV–Vis spectrophotometer (model UV-1602 Biomedical sciences), and a hotplate stirrer (model DAIHAN LABTECH CO. LTD). UV light (254 nm) and titanium ruthenium oxide anode were provided by De Nora Brazil.

Photolytic dye degradation

The photolysis of the dye solution was carried in a Pyrex glass container comprising 400 mL of dye wastewater. The UV light (254 nm) was immersed in the middle of the reactor and the wastewater solution was stirred using a magnetic stirrer. During the photolytic assay, 1 mL aliquot was withdrawn at a predetermined time interval (I h) and analyzed using a spectrophotometer. The decolorization was estimated by a reduction in absorbance intensity at λ_{max} of the dyes. The effect of temperature (30–40 °C), time (1–6 h) and pH (3–12) on the photolysis was also investigated. The reaction pH was maintained using droplets of sulfuric acid (H_2SO_4) or ammonium hydroxide (NH_4OH).

Electrochemical dye degradation

The electrochemical degradation experiments were conducted in the 500 mL Pyrex glass vessel as represented in Figure 2. The anode (titanium ruthenium oxide, $Ti/Ru0.3Ti0.7O_2$) and a stainless steel cathode were dipped in the reactor. Both electrodes were adjusted side by side at a distance of 1 cm and 45 cm^2 territories of electrodes and dye solutions. The current density was applied using the DC power supply. Before every electrochemical experiment, the anode was activated using 0.05 M H_2SO_4 solution applied at 15 mA cm^{-2} for 15 min. The current density varied between 2–12 mA/cm^2 for erythrosine and 2–7 mA/cm^2 for Allura red. Throughout the trials, erythrosine, and Allura red dye solution (400 mL) was electrolyzed using diverse supportive electrolytes. The concentration of electrolyte $NaNO_3$, Na_2SO_4 0.1 mol L^{-1} and NaCl (0.02–0.1 mol L^{-1}) and pH range of 3–12 were utilized for improving the conductivity and reducing electrolysis time. NH_4OH and H_2SO_4 were used to adjust the pH of dye solutions. The response solution was refluxed constantly at 450 rpm using a magnetic stirrer to maintain a uniform grouping of salts. Aliquots of 1 mL were withdrawn from the reaction mixture after 1 min of the time interval and analyzed by a UV–Vis spectrophotometer. The entire examinations were carried out at ambient temperature. The percentage of electrochemical discoloration of dyes was determined using Equation (4).

$$\%\ \text{Degradation} = \frac{A_o - A_t}{A_o} \times 100 \tag{4}$$

where A_t is absorbance after time t min of electrolysis, A_0 is absorbance at time ~0 min at λ_{max} (Khan *et al.* 2016).

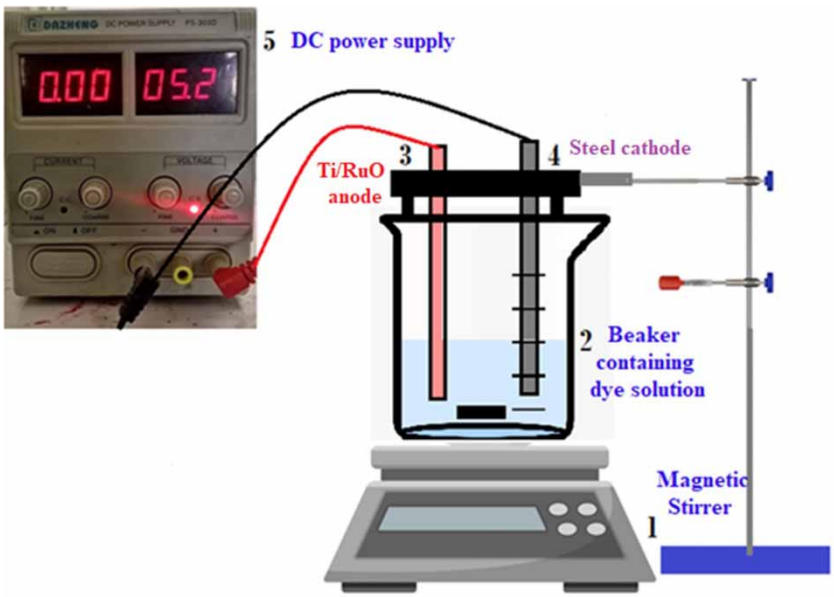

Figure 2 | Schematic representation of experimental setup for electrochemical degradation.

Downloaded from http://iwaponline.com/wst/article-pdf/81/5/971/768038/wst081050971.pdf
by guest

Statistical analysis and modeling

For the prediction of the relationship between the dependent variable (experimental results) and independent variables (experimental variables), empirical modeling techniques such as response surface methodology (RSM) is often utilized (Muhamad *et al.* 2018). Based on the statistically designed regression model of experimental data, RSM not only predicts the future response but also gives the opportunity to optimize it. Several types of design are available in RSM modeling, including central composite, Box–Behnken, user-defined, and historical data designs. In this study, historical data design was selected to evaluate the approximate function between dependent and independent variables in which design points are defined on the basis of existing experimental data without any limitation of the number of factors and levels compared to other RSM model designs (Jeirani *et al.* 2013; Muhamad *et al.* 2018).

RESULTS AND DISCUSSION

UV–Vis spectroscopy

The λ_{max} for both the dyes was determined with a wavelength scan range from 350–650 nm through a UV–Vis spectrophotometer. Allura red dye showed maximum absorption at 505 nm (Figure 3(a)), whereas the highest absorbance was recorded at 530 nm in the case of erythrosine dye (Figure 3(b)).

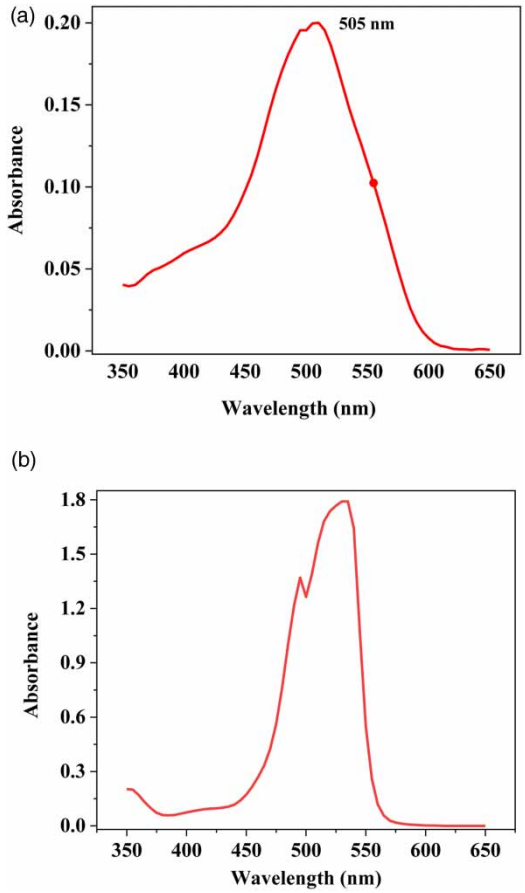

Figure 3 | λmax for (a) Allura red and (b) erythrosine dye using UV–Vis spectrophotometry.

Photolytic degradation of dyes

Impact of irradiation time on photolytic degradation

Irradiation duration exerts a noteworthy impact on the discoloration of dyes. The discoloration rate of photolysis increased by increasing the irradiation time. As the contact time of UV irradiation with dye increases, the degradation of dye increases, breaking the azo bonds and hence, results in high discoloration of dye. It can be observed from Figure 4(a) that the absorbance of Allura red dye (200 ppm) was reduced, resulting in 63.29% decolorization after exposure to 6 h UV illumination. Similarly, a substantial decrease in absorbance was also noticed for erythrosine dye (50 ppm) concomitant with 90.84% degradation after 6 h of UV radiation (Figure 4(b)). Hence, it was inferred that the degradation rate of dyes increased progressively with an increase in light span. Additionally, it is also revealed that the degree of dye degradation increases by extended interaction time of dye with UV light (Boucenna *et al.* 2019). The photolysis showed that the erythrosine dye is more stable than Allura red dye. Due to this reason, the concentration of Allura red (200 ppm) and erythrosine dye (50 ppm) was used in the experiments carried out for photolysis and electrochemical degradation.

Effect of pH on photolytic degradation

Figure 5(a) demonstrates that 35.24% decolorization of Allura red was achieved at pH 5.0. With an increase in solution pH to 6.0, the photolysis of dye was enhanced to 55% and maximum removal of dye up to 95.3% occurred at pH 12 after 1 h exposure to UV light. Consequently, it is presumed that an increase in pH prompts an increase in discoloration ability. For erythrosine dye, 90.84% decolorization was achieved at pH 6.0 after 6 h of irradiation time, and a further increase in pH values gave a diminished color removal (Figure 5(b)) (Wu *et al.* 2019). The photolysis

Downloaded from http://iwaponline.com/wst/article-pdf/81/5/971/768038/wst081050971.pdf
by guest

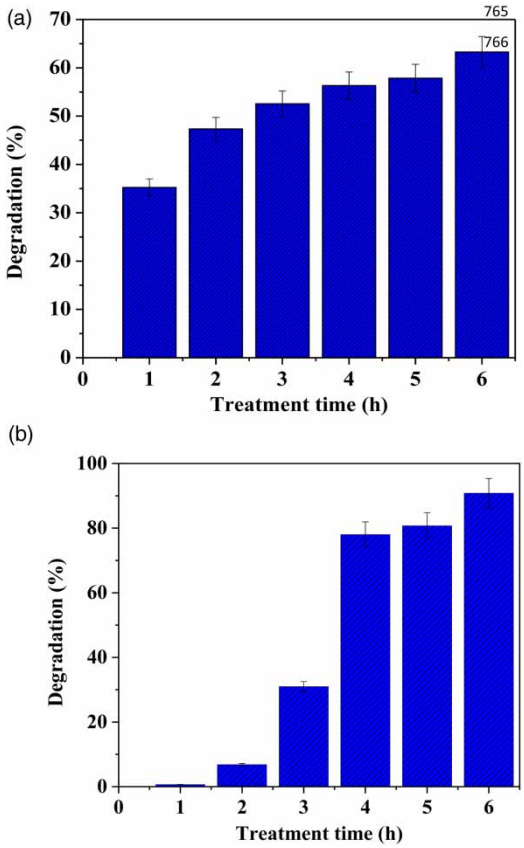

Figure 4 | Effect of irradiation time on photolysis of (a) Allura red and (b) erythrosine dye.

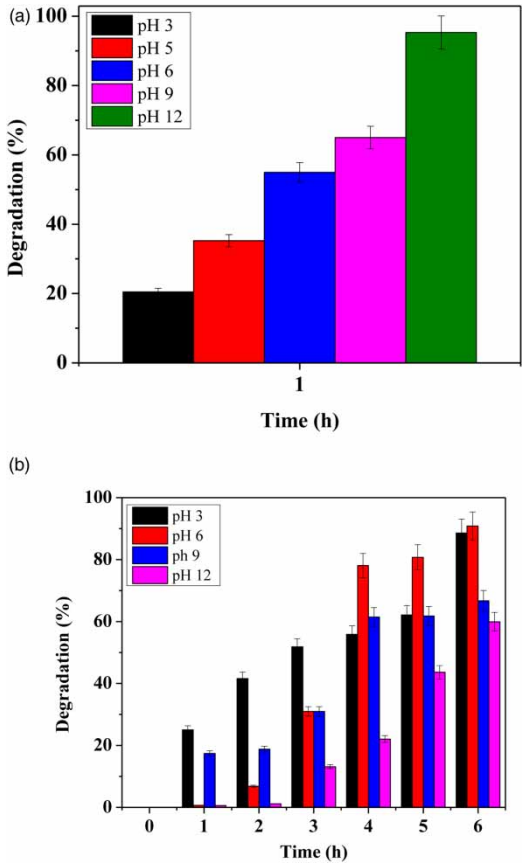

Figure 5 | Influence of pH on the degradation of (a) Allura red and (b) erythrosine dye.

of both the dyes increased when the pH of the solution was changed from highly acidic to slightly acid or alkaline. With an increase in pH, the time of photolysis was decreased. However, when in aqueous alkaline solution in the presence of UV irradiation the highly reactive hydroxyl radical is formed due to reactions with oxygen, which results in the degradation of Allura red dye. Without the presence of oxygen, the degradation of dye was prevented, suggesting that the presence of oxygen is important for the production of reactive radical species. Thus, the photolysis of Allura red dye in basic media could be preceded via direct reactions of the dye with highly reactive radical species formed in the presence of UV irradiation, as already reported in the literature (Soltani & Entezari 2013).

Impact of temperature on photolytic degradation

The effect of temperature during the erythrosine and Allura red dyes discoloration was examined with a temperature range varying from 30 to 40 °C for 1 h. A high degradation rate of 95.69% was achieved at 35 °C as depicted in Figure 6(a). Photolysis of Allura red dye increased by enhancing the temperature to 35 °C and diminished gradually with further enhancement in temperature up to 40 °C. A similar inclination occurred for 4-chloro-2-aminophenol utilizing joined procedures like hydrodynamic cavitation, UV photolysis, and ozone at temperature (30–38 °C), where the highest discoloration was accomplished at 35 °C (Wang *et al.* 2019). During the photolytic discoloration of erythrosine dye, the effective results were attained at 30 °C and diminished subsequently with a temperature rise after 6 h (Figure 6(b)). It implies that there is not much impact of temperature on photolytic removal of color and a rise in temperature from 32 to 40 °C poses no significant impact on the photolytic discoloration of methylene blue dyes. It means that UV light and oxygen has a major role in the photolysis of these dyes, which produces reactive radicals necessary for the process. The photolysis will stop in the absence of any of them (Soltani & Entezari 2013). However, temperature has a small role in photolysis and followed the same trend as reported earlier by Soltani & Entezari (2013). The photolysis of methylene blue dye, by increasing the temperature to 40 °C , has no effect on dye degradation. In an inert environment

Downloaded from http://iwaponline.com/wst/article-pdf/81/5/971/768038/wst081050971.pdf
by guest

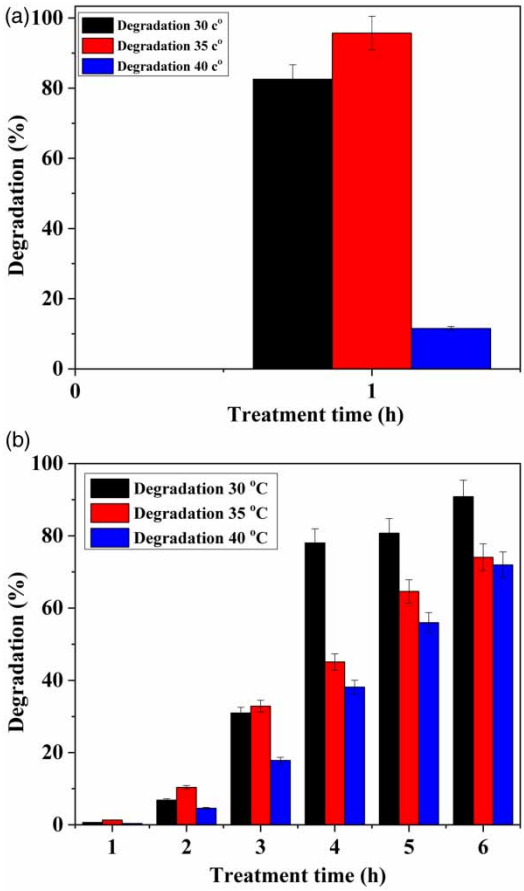

Figure 6 | Effect of temperature on photolysis of (a) Allura red and (b) erythrosine dye.

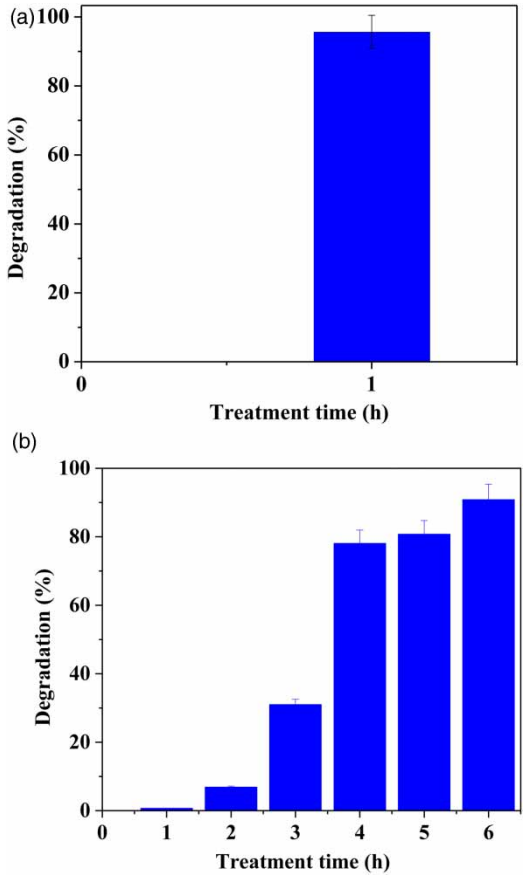

Figure 7 | Photolysis of (a) Allura red at pH 12, 35 °C and (b) erythrosine at pH 6, 30 °C.

(Ar atmosphere) the photolysis was completely stopped and under solar irradiation at the air atmosphere completed within 90 min (Soltani & Entezari 2013).

Photolytic degradation of dyes under optimized environment

UV spectra represents a high degradation of Allura red dye (95.69%) after 1 h treatment at pH 12 and 35 °C (Figure 7(a)). On the other hand, the greatest dye discoloration of 90.84% was achieved for erythrosine dye under the optimized conditions of pH 6.0 and 30 °C after 6 h exposure to UV light (Figure 7(b)). In a recent report, Soltani & Entezari (2013) observed the complete photolysis of methylene blue dye within 30 min at pH 12 and 32 °C.

Electrochemical degradation of dyes

The main purpose of the electrochemical method is to direct an electric flow through electrodes, bringing about various compound responses. By using a reducing agent, a conventional strategy is replaced by an inventive cathodic electron exchange (electrons are utilized, rather than synthetic compounds). An electrochemical cell is used to carry out the oxidation process. The dyeing mechanical assembly is coupled to the electrochemical cell and the dye bath is adequately diminished through an electrochemical procedure. The elements that influence electrochemical implementation include current density, structure geometry, type, number and dispersing of electrodes utilized, pH, temperature, and nature of the electrolyte, etc.

Impact of current density on electrochemical degradation

Electrochemical degradation of Allura red dye was carried out at the current flow of 2–7 mA cm^{-2} with different parameters remaining constant (Figure 8(a)). The degradation rate increases by increasing the current density. The ideal current density of 5 mA cm^{-2} was chosen for greater coloring removal and most minimal costs of vitality, in light of the

Downloaded from http://iwaponline.com/wst/article-pdf/81/5/971/768038/wst081050971.pdf
by guest

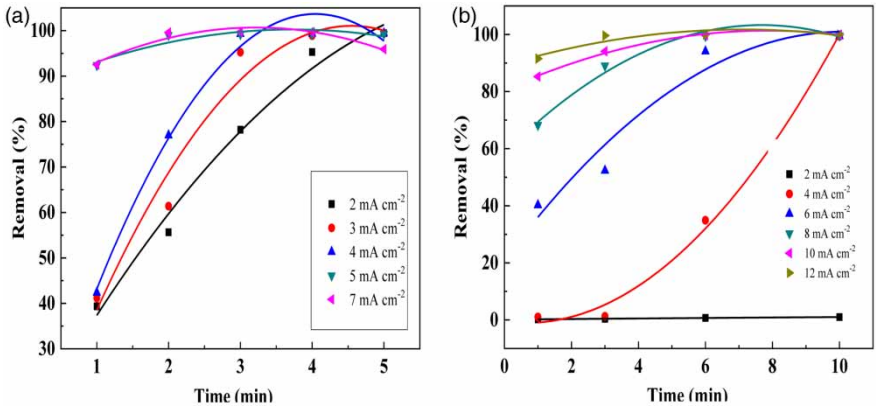

Figure 8 | Influence of current density on the degradation of (a) Allura red and (b) erythrosine dye.

a further increment in current density did not have any critical impact on dye discoloration. According to previously reported literature, the discoloration of reactive blue 19 dye at titanium-based DSA anode expanded directly with expanding ebb and flow densities (7.22–36.10 mA cm^{-2}) and with NaCl as an electrolyte (Baddouh *et al.* 2018). Therefore, the extraordinary current flow of 2–12 mA cm^{-2} was used to contemplate the proficiency of erythrosine dye's electrochemical removal with 0.1 mol L^{-1} NaCl at pH 6. The degradation efficiency noticeably increases with expanding current density in the range of 2–12 mA cm^{-2} (Figure 8(b)). The electrochemical decontamination of between 1 and 100% was achieved at 8 mA cm^{-2} after 10 min of electrolysis. With an increase in current density, the release of Cl/HClO was enhanced in NaCl electrolyte solution, leading to increased dye elimination (Jager *et al.* 2018). Hence, the ideal current flow for this situation was set as 8 mA cm^{-2} to reduce costs of energy and high dye removal. Siedlecka *et al.* (2018) investigated the removal of acid black 210 at BDD anode and found that discoloration efficiency of dye increased with increases in the ebb and flow densities from 25 to 100 mA cm^{-2}.

Impact of pH on electrochemical degradation

The influence of pH was evaluated on dye degradation with different variables being consistent, as shown in Figure 9. For Allura red, high degradation efficiency (99.60%) was observed at pH within 5 min electrolysis treatment. The electrochemical discoloration rate decreased with an increment in the pH of the mixture, as shown in Figure 9(a). The Allura red dye demonstrates greater discoloration in the acidic medium compared to the basic solution (3.86%) at pH 12, leading to a decrease in Cl_2/Cl^- production.

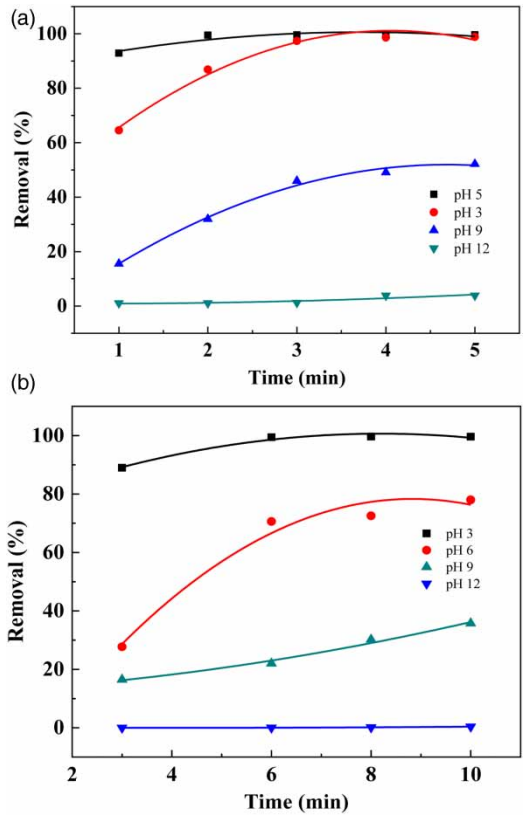

Figure 9 | Influence of pH on the electrochemical degradation of (a) Allura red and (b) erythrosine dye.

Along these lines, further analysis was done at pH 5.0. Sajid *et al.* (2018) achieved 70% discoloration of wastewater at pH 4 after 120 min of electrolysis. The impact of various pH on erythrosine dye's electrochemical degradation is shown in Figure 9(b). A degradation of 78.02% occurred after 6 min at pH 3.0, which increased to 99.61% at pH 6.0. The effectiveness of erythrosine discoloration was

Downloaded from http://iwaponline.com/wst/article-pdf/81/5/971/768038/wst081050971.pdf
by guest

reduced at higher pH, which demonstrates that the removal of erythrosine was higher using the acidic dye solution. In this way, the pH 6.0 was chosen as an ideal pH for analysis. In acidic dye solution, the Cl^- is present as HClO in the mixture and has a higher oxidation potential (1.49 V) than OCl^- (0.94 V) (García-Espinoza *et al.* 2018) due to the fact that in basic medium, the OCl^- is present, which produces low degradation at higher pH.

Impact of supporting electrolytes on electrochemical degradation

Figure 10(a) and 10(b) show the electrochemical degradation of erythrosine and Allura red dye utilizing different supporting electrolytes. It is revealed that with the availability of Na_2SO_4 and $NaNO_3$ electrolytes, a color removal of 9.27% and 6.42% was acquired after 5 min of electrolysis separately for Allura red (Figure 10(a)), and 0.389% and 0.222% was acquired following 10 min reflux for erythrosine dye (Figure 10(b)). The presence of SO_4^- and NO_3^- causes direct electrochemical oxidation and the cathode showed weak electrocatalytic performance because of the absence of Cl^- and the possibility of electrode debasement that leads to the development of a fixed layer on anode exterior. The dyes could not be oxidized using SO_4^- and NO_3^- as electrolytes using direct oxidation process. A 99.60% degradation was achieved, using NaCl among other supporting electrolytes, after 5 min of electrolytic treatment for Allura red and 99.61% erythrosine dye removal was achieved after 10 min of electrolysis (Figure 10(b)). This is the result of the generation of the high level of Cl_2/OCl^- species on the working electrode (anode) exterior leading to indirect oxidation. In indirect oxidation, the wastewater containing Cl^- is converting into HClO oxidant species, which are produced eclectically on the anode surface and its proposed mechanism is given in Equations (7)–(10).

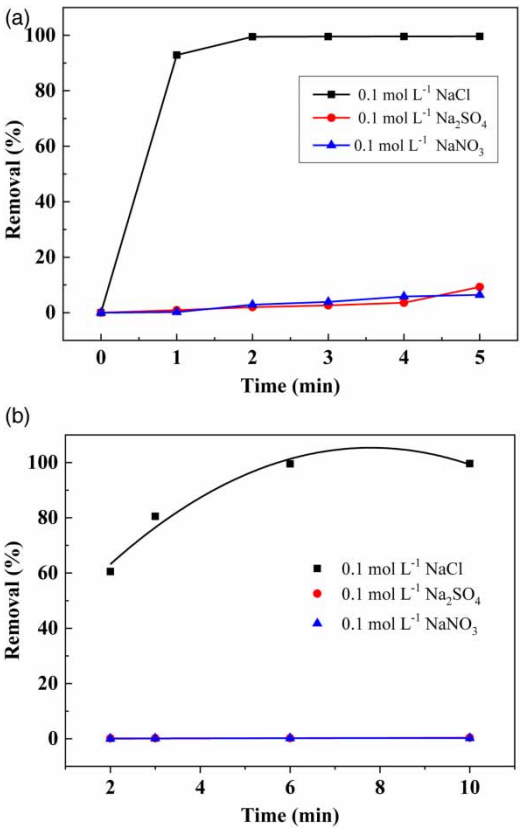

Figure 10 | Influence of electrolyte concentration on the degradation of (a) Allura red and (b) erythrosine dye.

$$\text{Anode Reaction } 2Cl^- \rightarrow Cl_2 + 2e^- \quad (5)$$

$$\text{Cathode Reaction } 2H_2O + 2e^- \rightarrow H_2 + 2OH^- \quad (6)$$

$$\text{Solution } Cl_2 + H_2O \rightarrow HClO + HCl \quad (7)$$

$$HClO \rightarrow H^+ + OCl^- \quad (8)$$

It is obvious that NaCl was observed as the best electrolyte for both Allura red and erythrosine dyes based on its greater removal efficiency. Referring to the previous reports, the pesticides are completely degraded at 0.1 mol L^{-1} of NaCl within 60 min of electrolysis process (Zhu *et al.* 2018).

Impact of NaCl concentration on electrochemical degradation

The impact of NaCl concentrations on Allura red dye degradation was examined under a consistent current flow of 5 mA cm^{-1} after 5 min of electrolysis, and responses are presented in Figure 11(a). With the increase in NaCl concentration, the removal efficiency of dye also increases. The greatest discoloration (99.60%) was achieved with 0.1 mol L^{-1} NaCl, and therefore the same concentration of NaCl was utilized throughout the test work. Figure 11(b) portrays the impact of various concentrations of NaCl on the electrochemical discoloration effectiveness of erythrosine dye. The lowest (18.51%) and the highest (99.61%) discoloration was recorded at 0.02 and 0.1 mol L^{-1} of NaCl after 10 min under the consistent current flow of 8 mA cm^{-2}. Thus, further analysis was done with 0.1 mol L^{-1} of NaCl electrolyte. A comparison was made with a previous report where the almost complete

Downloaded from http://iwaponline.com/wst/article-pdf/81/5/971/768038/wst081050971.pdf
by guest

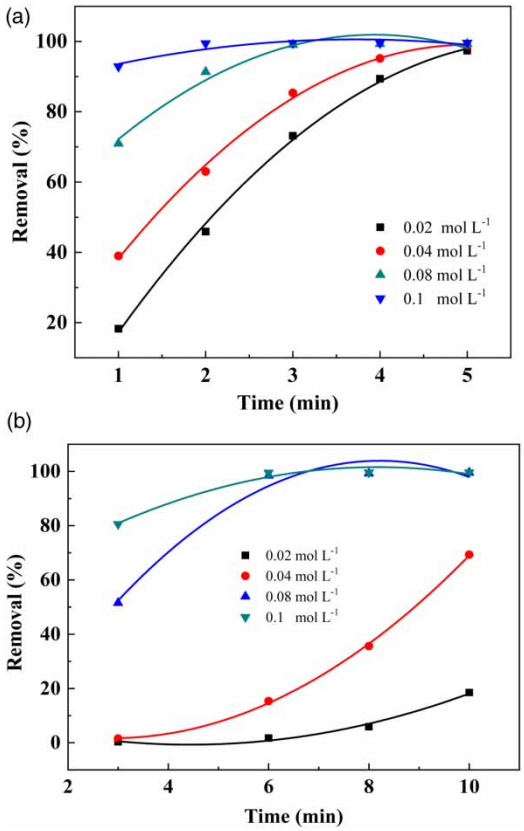

Figure 11 | Effect of NaCl concentration on the degradation of (a) Allura red and (b) erythrosine dye.

discoloration (95.1%) of tartrazine E102 dye was noted utilizing carbon/lead dioxide anodes after 10 min with NaCl (Hamad *et al.* 2018). The electrochemical degradation pattern of Allura red dye in NaCl using a BDD electrode (Thiam *et al.* 2015) gave a benzenic derivative due to breaking of (–N = N–) of the dye molecule. The hydroxylation, demethylation, and carboxylation along with the chlorination reactions occurred, resulting in primary aromatic compounds. The chloro-derivatives are formed due to active chlorine. These compounds were removed as the electrolysis proceeded. Jain *et al.* (2005) proposed the electrochemical degradation pathway of erythrosine dye. After the electrolysis of erythrosine dye, the chemical oxygen demand value decreased significantly compared to the original dye solution.

Calculation of energy consumption

Energy utilization is a prime element used to evaluate the feasibility of the electrochemical degradation process. The expense of energy consumed was estimated using Equation (9):

$$\text{Energy Consumption (kWm}^{-3}) = \frac{I \times V \times t}{Vs} \quad (9)$$

where t is the electrolysis time (h), V is an average voltage (V), I is the current density (A) and Vs is the volume (m^3) of solution used. Table 1 illustrates the electrochemical discoloration of Allura red dye with concentrations of 200 ppm at various current flows (2–7 mA cm^{-2}). Notably, as the current flow increases from 2 to 7 mA cm^{-2}, the energy utilization was enhanced from 0.065 to 0.366 kWh m^{-3}. This shows that the expenditure of energy at 2 mA cm^{-2} is much less than 7 mA cm^{-2}. However, the process of discoloration increases at greater current flow, which might be due to the enlarged evolution reaction of H_2 and O_2. Thus, it is concluded that the minimum calculated energy consumption at an optimum applied current density of 5 mA cm^{-2} was 0.196 kWh m^{-3} for maximum discoloration and for the least energy charge due to the shorter time. Similarly, Alcocer *et al.* (2018) reported that the minimum electrical energy consumption for methyl orange was 1.11 kWh m^{-3} at 5 mA current density. Table 2 presents the electrical energy utilization possibilities or the electrochemical discoloration of erythrosine dye (50 ppm) at various current densities (4–12 mA cm^{-2}). For erythrosine dye, the minimal electrical energy utilization was 0.941 kWh m^{-3} at the optimum current flow of 8 mA cm^{-2} for maximum degradation for the least energy charge due to the shorter time. This significant result adds immense worth toward this effort as a vital reduction of energy, which is the main aspect affecting the working expenditure for such

Table 1 | Energy consumption calculations for the degradation of Allura red dye

Parameters		Time (h)	Average voltage (V)	Energy consumption (kWh m^{-3})
Current density (mA cm^{-2})	2	0.083	3.44	0.065
	3	0.083	4.3	0.120
	4	0.083	4.4	0.168
	5	0.083	4.24	0.196
	7	0.083	5.58	0.366
Electrolytes	Na_2SO_4	0.083	4.0	0.186
	$NaNO_3$	0.083	4.8	0.224
	NaCl	0.083	4.24	0.196
NaCl (mol L^{-1})	0.02	0.083	3.94	0.186
	0.04	0.083	4.22	0.200
	0.08	0.083	4.7	0.224

Downloaded from http://iwaponline.com/wst/article-pdf/81/5/971/768038/wst081050971.pdf
by guest

Table 2 | Energy consumption calculations for the decontamination of erythrosine

Parameters		Time (h)	Average voltage (V)	Energy consumption (kWh m^{-3})
Current density (mA cm^{-2})	2	0.166	3.3	0.123
	4	0.166	4.2	0.298
	6	0.166	5.2	0.582
	8	0.166	6.2	0.941
	10	0.166	7.1	1.325
	12	0.166	7.96	1.770
Electrolytes	Na_2SO_4	0.166	4.8	0.717
	$NaNO_3$	0.166	6.46	0.971
	NaCl	0.166	6.2	0.941
NaCl (mol L^{-1})	0.02	0.166	5.06	0.304
	0.04	0.166	5.33	0.806
	0.08	0.166	6.1	0.926

an application. Similarly, during the sulfamethoxazole ($C_{10}H_{11}N_3O_3S$) degradation, the applied current density is between 5 and 10 mA cm^{-2} due to less energy consumption and less time (Nidheesh *et al.* 2018) (Tables 1 and 2).

From the above discussion, a brief comparison of electrochemical and photolytic degradation procedures can be deduced. In the case of photolytic degradation, up to 90% of degradation was obtained at the cost of high-energy consumption. While in the case of electrochemical degradation, 100% results were obtained with low cost, cheap equipment, more feasibility, and more accuracy. Hence, the latter was found to be the most effective method for the degradation of both tested dyes.

Statistical analysis and modeling

Based on the historical data, optimization of the treatment parameters of Allura red and erythrosine for electrochemical oxidation was performed by RSM using statistical software package MINITAB. Custom data analysis option was utilized, which is similar to the custom design historical data available in statistical software package DESIGN EXPERT. The first step in RSM is to determine a mathematical equation that describes the functional relationship between response/dependent variables Y (in this case, Allura red and erythrosine dyes) and a set of independent variables X (in this case, these are operating parameters such as time, pH, current density, and NaCl concentration). The mathematical expression of the response could be a first-order, second-order, or cubical model, which fits well in the region of the independent variables. Regression analysis was applied to build an adequate model for each response factor and the goodness-of-fit and statistical significance of the models were assessed by analysis of variance (ANOVA) for 95% confidence interval (Anderson & Whitcomb 2015). The design matrix of the four independent variables in the uncoded form based on previous experiments is presented in Table 3 and Tables S1 and S2 (Supplementary Information), along with the predicted and experimental values of the responses (Allura red and erythrosine dye removal). The predicted values of the responses were obtained from the quadratic model-fitting techniques for the percentage of Allura red dye removal and erythrosine dye. The corresponding quadratic polynomial Equations (10) and (11) are obtained based on the experimental results.

$$\begin{aligned}\textbf{Allura Red Removal}\ (\%) = {} & -89.1 + 61.98^{*}\text{Time} - 12.63^{*}\ \text{pH} + 1503^{*}\text{NaCl} \\ & + 27.97^{*}\text{Current} - 2.68^{*}\text{Time}^2 + 0.021^{*}\ \text{pH}^2 \\ & - 5182^{*}\text{NaCl}^2 - 1.150^{*}\text{Current}^2 - 0.228^{*}\text{Time}^{*}\ \text{pH} \\ & - 175.6^{*}\text{Time}^{*}\text{NaCl} - 4.377^{*}\text{Time}^{*}\text{Current}\end{aligned} \tag{10}$$

$$\begin{aligned}\textbf{Erythrosine Removal}\ (\%) = {} & -248 + 20.60^{*}\text{Time} + 12.3^{*}\ \text{pH} + 3449^{*}\text{NaCl} \\ & + 14.0^{*}\text{Current} + 0.025^{*}\text{Time}^2 - 1.985^{*}\ \text{pH}^2 \\ & - 13937^{*}\text{NaCl}^2 - 0.195^{*}\text{Current}^2 - 0.206^{*}\text{Time}^{*}\ \text{pH} \\ & - 90.0^{*}\text{Time}^{*}\text{NaCl} - 0.893^{*}\text{Time}^{*}\text{Current}\end{aligned} \tag{11}$$

To test the adequacy and validity of the second-order model, ANOVA was performed as shown in Table 4. The high F-value of the models (i.e. 88.2 for Allura red and 15.4 for erythrosine) are higher than for Fisher Table (2.424 for a 95% coefficient level), demonstrating that the model is fit to the experimental results (Zhang *et al.* 2018). Moreover, linear, self-interaction, and two-way

Table 3 | Experimental levels and ranges of individual variables for Allura red and erythrosine dye degradation process

	Allura red			Erythrosine dye		
	Levels			Levels		
Parameters	−1	0	1	−1	0	1
Time (min)	1	3	5	1	5.5	10
pH	4	8	12	3	6	12
NaCl (moL^{-1})	0.02	0.06	0.1	0.02	0.06	0.1
Current density (mA cm^{-2})	2	4.5	7	2	9	12

Downloaded from http://iwaponline.com/wst/article-pdf/81/5/971/768038/wst081050971.pdf
by guest

Table 4 | ANOVA of the parameters for Allura red and erythrosine dye removal efficiency

	Allura red removal efficiency (%)					Erythrosine removal efficiency (%)				
Term	**DF**	**Adj SS**	**Adj MS**	**F-value**	***p*-value**	**DF**	**Adj SS**	**Adj MS**	**F-value**	***p*-value**
Model	**11**	54,710	**4,973.7**	**88.02**	**0**	**11**	**31,643.6**	**2,876.69**	**15.49**	**0**
Linear	4	43,111.6	10,777.9	190.74	0	4	19,909	4,977.25	26.8	0
Time	1	5,685.8	5,685.8	100.62	0	1	2,027.4	2,027.38	10.92	0.003
pH	1	34,325.3	34,325.3	607.47	0	1	7,593.9	7,593.92	40.9	0
NaCl	1	3,367.4	3,367.4	59.59	0	1	8,303.6	8,303.62	44.72	0
Current	1	888	888	15.72	0	1	1,218.6	1,218.55	6.56	0.018
Square	4	1,396.8	349.2	6.18	0.001		1,691.1	422.78	2.28	0.095
Time*Time	1	897.3	897.3	15.88	0	1	0.9	0.86	0	0.946
pH*pH	1	0.3	0.3	0.01	0.943	1	922.9	922.95	4.97	0.037
NaCl*NaCl	1	220.5	220.5	3.9	0.05	1	497.9	497.89	2.68	0.116
Current*Current	1	229.4	229.4	4.06	0.05	1	7.9	7.94	0.04	0.838
Two-Way Interaction	3	3,428.6	1,142.9	20.23	0		1,142.7	380.89	2.05	0.137
Time*pH	1	20.6	20.6	0.36	0.549	1	12.4	12.39	0.07	0.799
Time*NaCl	1	1,762.5	1,762.5	31.19	0	1	726.8	726.79	3.91	0.061
Time*Current	1	1,606.3	1,606.3	28.43	0	1	345.2	345.17	1.86	0.187
		$R^2 = 0.9584$		$R^2(Adj) = 0.9475$			$R^2 = 0.8903$		$R^2(Adj) = 0.8328$	

interactions among the variables are significant as in most cases $p < 0.05$. A good presentation of coefficient of determination for Allura red (R^2: 0.9584) implies that 95.84% of variables are explained by the model, whereas only 4.16% of variables could not be explained, and 89.03% in case of erythrosine dye (Figure S1, Supplementary Information).

The interaction effects of time, pH, NaCl concentration, and current density on removal efficiency of Allura red is presented in Figure S2(a)–S2(e), which shows the variation in removal rate when two parameters are varied while the remaining two parameters hold at mean values according to Table 3. It is evident that in all cases, a higher removal rate is achieved at lower pH values in the tested range, while the other parameters were varied between their low to upper range. Similar criteria were set to evaluate the interaction effect of various variables on the degradation efficiency of erythrosine dye as shown in Figure S3(a)–S3(e), which shows that accelerated removal rates are achieved at low pH values, higher NaCl concentrations, and elevated current densities.

To see the effect of individual parameters and their interaction on the electrochemical decolorization process, Pareto analysis was performed. The percentage of input variables on the Allura red and erythrosine dye degradation rate was evaluated according to Pareto analysis according to Equation (12) (Khataee *et al.* 2010):

$$P_i = \frac{\beta_i^2}{\sum \beta_i^2} \times 100 \quad (i \neq 0) \tag{12}$$

Figure S4 presents the Pareto chart of standardized effect for a percentage of Allura red removal, which shows that all four input variables have a significant influence on the decay efficiency of Allura red. Among all four operating parameters, pH (70.04%) and electrolysis time (11.60%) are the main factors on the Allura red degradation efficiency, while the contribution of individual factors for erythrosine degradation was found in the order: NaCl > pH > time > current density (Figure S5).

The optimized conditions for Allura red and erythrosine dye removal were determined by the response optimizer. The aim was set as 'maximize' to obtain the maximum degradation efficacy of Allura red and determine the optimum operating conditions. Many solutions/operating conditions are available to achieve maximized degradation efficiency of Allura red and erythrosine dye (Tables S3 and S4), and one representative solution for Allura red degradation is presented in Figure S6, which shows that the highest Allura red degradation efficiency (100%) was achieved at 1.95 min, pH 5.05, NaCl concentration of 0.1 mol/L, and applied current of 7 mA. However,

Downloaded from http://iwaponline.com/wst/article-pdf/81/5/971/768038/wst081050971.pdf
by guest

many solutions are available that have the desired removal efficiency where operating parameters vary between their upper and lower limits to achieve the same target. It is interesting to see that >95% decay rate is only achieved when pH varies between 4 and 5, which is in accordance with the Pareto chart indicating that pH is the most influential parameter (Table S4). In Table S4, the selection criteria for the best operating condition should be based on minimum energy consumption together with accelerated and desired removal rates.

CONCLUSION

In this study, the photolytic and electrochemical degradation of erythrosine and Allura red dyes have been evaluated. Critical parameters that affect these processes, such as pH, temperature, supporting electrolytes, NaCl concentration, and current density, were optimized for maximum discoloration efficiency. The following conclusions can be drawn from the study:

- The photolytic process was slow and degraded 95.69% Allura red in 1 h and took 6 h to degrade erythrosine up to 90.84%. Solution pH and temperature has an influence on the rate of degradation.
- Photolytic degradation mainly involves the breaking of bonds due to the absorption of UV radiation and hydroxyl radical produced in an aqueous medium.
- Electrochemical degradation using Ti/Ru0.3Ti0.7O_2 anode was fast and degraded erythrosine and Allura red dye in 10 and 5 min, respectively.
- The electrochemical degradation of Allura red and erythrosine was strongly influenced by pH and NaCl concentration and moderately affected by current density.
- The electrochemical process mainly involves indirect oxidation of dyes in the bulk of solution, and the reactive chlorine species, such as Cl_2, HClO, ClO^-, are generated on the anode surface and oxidize the dye molecules in solution.
- The high removal efficiency and fast degradation rate demonstrate the electrochemical process as an alternative to treat wastewater containing food dyes.

ACKNOWLEDGEMENTS

All listed authors are grateful to their representative departments and universities for the financial support and analytical services used in this study.

CONFLICT OF INTEREST

The authors declare that they have no conflict of interest.

SUPPLEMENTARY MATERIAL

The Supplementary Material for this paper is available online at https://dx.doi.org/10.2166/wst.2020.182.

REFERENCES

Alcocer, S., Picos, A., Uribe, A. R., Perez, T. & Peralta-Hernandez, J. M. 2018 Comparative study for degradation of industrial dyes by electrochemical advanced oxidation processes with BDD anode in a laboratory stirred tank reactor. *Chemosphere* **205**, 682–689.

Ali, N., Kamal, T., Ul-Islam, M., Khan, A., Shah, S. J. & Zada, A. 2018 Chitosan-coated cotton cloth supported copper nanoparticles for toxic dye reduction. *International Journal of Biological Macromolecules* **111**, 832–838.

Ali, N., Zaman, H., Bilal, M., Nazir, M. S. & Iqbal, H. M. 2019 Environmental perspectives of interfacially active and magnetically recoverable composite materials–A review. *Science of the Total Environment.* **670**, 523–538.

Ali, N., Khan, A., Nawaz, S., Bilal, M., Malik, S., Badshah, S. & Iqbal, H. M. 2020 Characterization and deployment of surface-engineered chitosan-triethylenetetramine nanocomposite hybrid nano-adsorbent for divalent cations decontamination. *International Journal of Biological Macromolecules* **152**, 663–671.

Al-Shabib, N. A., Khan, J. M., Malik, A., Sen, P., Ramireddy, S., Chinnappan, S., Alamery, S. F., Husain, F. M., Ahmad, A., Choudhry, H., Khan, M. I. & Shahzad, S. A. 2019 Allura red rapidly induces amyloid-like fibril formation in hen egg-white lysozyme at physiological pH. *International Journal of Biological Macromolecules* **127**, 297–305.

Anderson, M. & Whitcomb, P. 2015 *DOE Simplified*, 2nd edn. Productivity Press, New York.

Asfaram, A., Ghaedi, M., Abidi, H., Javadian, H., Zoladl, M. & Sadeghfar, F. 2018 Synthesis of Fe_3O_4@CuS@Ni_2P-CNTs magnetic nanocomposite for sonochemical-assisted sorption and pre-concentration of trace Allura Red from aqueous samples prior to HPLC-UV detection: CCD-RSM design. *Ultrasonics – Sonochemistry* **44**, 240–250.

Aziz, A., Ali, N., Khan, A., Bilal, M., Malik, S., Ali, N. & Khan, H. 2020 Chitosan zinc sulfide nanoparticles, characterization and their photocatalytic degradation efficiency for azo dyes. *International Journal of Biological Macromolecules* **153**, 502–512.

Baddouh, A., Bessegato, G. G., Rguiti, M. M., El-Ibrahimi, B., Bazzi, L., Hilali, M. & Zanoni, M. V. B. 2018 Electrochemical decolorization of Rhodamine B dye: influence of anode material, chloride concentration and current density. *Journal of Environmental Chemical Engineering* **6**, 2041–2047.

Downloaded from http://iwaponline.com/wst/article-pdf/81/5/971/768038/wst081050971.pdf
by guest

Bendjama, H., Merouani, S., Hamdaoui, O. & Bouhelassa, M. 2019 UV-photolysis of Chlorazol Black in aqueous media: process intensification using acetone and evidence of methyl radical implication in the degradation process. *Journal of Photochemistry & Photobiology A: Chemistry* **368**, 268–275.

Bilal, M., Rasheed, T., Iqbal, H. M., Li, C., Wang, H., Hu, H. & Zhang, X. 2018a Photocatalytic degradation, toxicological assessment and degradation pathway of CI Reactive Blue 19 dye. *Chemical Engineering Research and Design* **129**, 384–390.

Bilal, M., Rasheed, T., Iqbal, H. M., Hu, H., Wang, W. & Zhang, X. 2018b Toxicological assessment and UV/TiO_2-based induced degradation profile of reactive black 5 dye. *Environmental Management* **61** (1), 171–180.

Bilal, M., Rasheed, T., Sosa-Hernández, J. E., Raza, A., Nabeel, F. & Iqbal, H. 2018c Biosorption: an interplay between marine algae and potentially toxic elements – a review. *Marine Drugs* **16** (2), 65.

Boucenna, A., Oturan, N., Chabani, M., Bouafia-Chergui, S. & Oturan, M. A. 2019 Degradation of Nystatin in aqueous medium by coupling UV-C irradiation, H_2O_2photolysis, and photo-Fenton processes. *Environmental Science and Pollution Research* **26**, 23149–23161.

García-Espinoza, J. D., Mijaylova-Nacheva, P. & Aviles-Flores, M. 2018 Electrochemical carbamazepine degradation: effect of the generated active chlorine, transformation pathways, and toxicity. *Chemosphere* **192**, 142–151.

Gnanasekaran, L., Hemamalini, R., Rajendran, S., Qin, J., Yola, M. L., Atar, N. & Gracia, F. 2019 Nanosized Fe_3O_4 incorporated on a TiO_2 surface for the enhanced photocatalytic degradation of organic pollutants. *Journal of Molecular Liquids* **287**, 110967.

Hamad, H., Bassyouni, D., El-Ashtoukhy, E., Amin, N. & El-Latif, M. A. 2018 Electrocatalytic degradation and minimization of specific energy consumption of synthetic azo dye from wastewater by anodic oxidation process with an emphasis on enhancing economic efficiency and reaction mechanism. *Ecotoxicology and Environmental Safety*. **148**, 501–512.

Jager, D., Kupka, D., Vaclavikova, M., Ivanicova, L. & Gallios, G. 2018 Degradation of Reactive Black 5 by electrochemical oxidation. *Chemosphere* **190**, 405–416.

Jain, R., Bhargava, M. & Sharma, N. 2005 Electrochemical degradation of erythrosine dye in pharmaceutical and food product industries effluent. *Journal of Scientific and Industrial Research*, **64**, 191–197.

Jeirani, Z., Jan, B. M., Ali, B. S., Noor, I., See, C. & Saphanuchart, W. 2013 Prediction of the optimum aqueous phase composition of a triglyceride microemulsion using response surface methodology. *Journal of Industrial and Engineering Chemistry* **19** (4), 1304–1309.

Khan, H., Khalil, A. K., Khan, A., Saeed, K. & Ali, N. 2016 Photocatalytic degradation of bromophenol blue in aqueous medium using chitosan conjugated magnetic nanoparticles. *Korean Journal of Chemical Engineering* **33**, 2802–2807.

Khan, A., Shah, S. J., Mehmood, K., Ali, N. & Khan, H. 2018 Synthesis of potent chitosan beads a suitable alternative for textile dye reduction in sunlight. *Journal of Materials Science: Materials in Electronics* **30** (1), 406–414.

Khan, A., Ali, N., Bilal, M., Malik, S., Badshah, S. & Iqbal, H. 2019a Engineering functionalized chitosan-based sorbent material: characterization and sorption of toxic elements. *Applied Sciences* **9** (23), 5138.

Khan, H., Khalil, A. K. & Khan, A. 2019b Photocatalytic degradation of alizarin yellow in aqueous medium and real samples using chitosan conjugated tin magnetic nanocomposites. *Journal of Materials Science: Materials in Electronics* **30** (24), 21332–21342.

Khataee, A. R., Zarei, M. & Moradkhannejhad, L. 2010 Application of response surface methodology for optimization of azo dye removal by oxalate catalyzed photoelectro-Fenton process using carbon nanotube-PTFE cathode. *Desalination* **258** (1), 112–119.

Liu, L., Bilal, M., Duan, X. & Iqbal, H. M. 2019 Mitigation of environmental pollution by genetically engineered bacteria – current challenges and future perspectives. *Science of The Total Environment* **667**, 444–454.

Martínez-Huitle, C. A. & Panizza, M. 2018 Electrochemical oxidation of organic pollutants for wastewater treatment. *Current Opinion in Electrochemistry* **11**, 62–71.

Mazloom, F., Ghiyasiyan-Arani, M., Monsef, R. & Salavati-Niasari, M. 2018 Photocatalytic degradation of diverse organic dyes by sol-gel synthesized $Cd_2V_2O_7$ nanostructures. *Journal of Materials Science: Materials in Electronics* **29**, 18120–18127.

Muhamad, M. S., Hamidon, N., Salim, M. R., Yusop, Z., Lau, W. J. & Hadibarata, T. 2018 Response surface methodology for modeling bisphenol a removal using ultrafiltration membrane system. *Water, Air, & Soil Pollution* **229** (7), 222.

Nakamura, K. C., Guimarães, L. S., Magdalena, A. G., Angelo, A. C. D., Andrad, A. R., Garcia-Segura, S. & Pipi, A. R. F. 2019 Electrochemically driven mineralization of Reactive Blue 4 cotton dye: on the role of in situ generated oxidants. *Journal of Electroanalytical Chemistry* **840**, 415–422.

Nidheesh, P. V., Zhou, M. & Oturan, M. A. 2018 An overview of the removal of synthetic dyes from water by electrochemical advanced oxidation processes. *Chemosphere* **197**, 210–227.

Ostovan, A., Asadollahzadeh, H. & Ghaedi, M. 2018 Ultrasonically synthesis of Mn- and Cu-@ZnS-NPs-AC based ultrasound-assisted extraction procedure and validation of a spectrophotometric method for a rapid preconcentration of Allura Red AC (e129) in food and water samples. *Ultrasonics – Sonochemistry* **43**, 52–60.

Rasheed, T., Bilal, M., Iqbal, H. M., Hu, H. & Zhang, X. 2017 Reaction mechanism and degradation pathway of rhodamine 6G by photocatalytic treatment. *Water, Air, & Soil Pollution* **228** (8), 291.

Rasheed, T., Bilal, M., Iqbal, H. M., Shah, S. Z. H., Hu, H., Zhang, X. & Zhou, Y. 2018a TiO_2/UV-assisted rhodamine B degradation: putative pathway and identification of intermediates by UPLC/MS. *Environmental Technology* **39** (12), 1533–1543.

Rasheed, T., Bilal, M., Li, C., Nabeel, F., Khalid, M. & Iqbal, H. M. 2018b Catalytic potential of bio-synthesized silver nanoparticles using *Convolvulus arvensis* extract for the

Downloaded from http://iwaponline.com/wst/article-pdf/81/5/971/768038/wst081050971.pdf
by guest

degradation of environmental pollutants. *Journal of Photochemistry and Photobiology B: Biology* **181**, 44–52.

Safni, S., Wahyuni, M. R., Khoiriah, K. & Yusuf, Y. 2019 Photodegradation of phenol using N-doped TiO_2 catalyst. *Molecule* **14**, 6–10.

Sahu, K., kuriakose, S., Singh, J., Satpati, B. & Mohapatra, S. 2018 Facile synthesis of ZnO nanoplates and nanoparticle aggregates for highly efficient photocatalytic degradation of organic dyes. *Journal of Physics and Chemistry of Solids* **121**, 186–195.

Sajid, M. M., Khan, S. B., Shad N, A. & Amin, N. 2018 Synthesis of $Zn_3(VO_4)_2$/$BiVO_4$heterojunction composite for the photocatalytic degradation of methylene blue organic dye and electrochemical detection of h_2o_2. *RSC Advances* **8**, 35403–35412.

Salazar, R., Ureta-Zanartu, M. S., Gonz-alez-Vargas, C., Brito, C. N. & Martinez-Huitle, C. A. 2018 Electrochemical degradation of industrial textile dye disperse yellow 3: role of electrocatalytic material and experimental conditions on the catalytic production of oxidants and oxidation pathway. *Chemosphere* **198**, 21–29.

Shetti, N. P., Malode, S. J., Malladi, R. S., Nargund, S. L., Shuklad, S. S. & Aminabhavid, T. M. 2019 Electrochemical detection and degradation of textile dye Congo red at graphene oxide modified electrode. *Microchemical Journal* **146**, 387–392.

Shi, X., Tian, A., You, J., Yang, H., Wang, Y. & Xue, X. 2018 Degradation of organic dyes by a new heterogeneous Fenton reagent – Fe2GeS4 nanoparticle. *Journal of Hazardous Materials* **353**, 182–189.

Siedlecka, E. M., Ofiarska, A., Borzyszkowska, A. F., Białk-Bielinska, A., Stepnowski, P. & Pieczynska, A. 2018 Cytostatic drug removal using electrochemical oxidation with BDD electrode: degradation pathway and toxicity. *Water Research* **144**, 235–245.

Soltani, T. & Entezari, M. H. 2013 Photolysis and photocatalysis of methylene blue by ferrite bismuth nanoparticles under sunlight irradiation. *Journal of Molecular Catalysis A: Chemical* **377**, 197–203.

Tiwari, B. & Ram, S. 2019 Biogenic synthesis of graphitic carbon nitride for photocatalytic degradation of organic dyes. *ACS Omega* **4**, 10263–10272.

Thiam, A., Sirés, I., Garrido, J. A., Rodríguez, R. M. & Brillas, E. 2015 Effect of anions on electrochemical degradation of azo dye Carmoisine (Acid Red 14) using a BDD anode and air-diffusion cathode. *Separation and Purification Technology* **140**, 43–52.

Vasconcelos, V. M., Ponce-de-León, C., Rosiwal, S. M. & Lanza, M. R. V. 2019 Electrochemical degradation of reactive blue 19 dye by combining boron-doped diamond and reticulated vitreous carbon electrodes. *Chem. Electro. Chem.* **6**, 3516–3524. https://doi.org/10.1002/celc.201900563.

Veisi, H., Razeghi, S., Mohammadi, P. & Hemmati, S. 2019 Silver nanoparticles decorated on thiol-modified magnetite nanoparticles (Fe_3O_4/SiO_2-Pr-S-Ag) as a recyclable nanocatalyst for degradation of organic dyes. *Materials Science & Engineering C* **97**, 624–631.

Wang, N. N., Hu, Q., Hao, L. L. & Zhao, Q. 2019 Degradation of Acid Organic 7 by modified coal by ash-catalyzed Fenton-like a process: kinetics and mechanism study. *International Journal of Environmental Science and Technology* **16**, 89–100.

Wu, C. H., Kuo, C. Y., Dong, C. D., Chen, C. W. & Lin, Y. L. 2019 Removal of sulfonamides from wastewater in the UV/TiO_2 system: effects of pH and salinity on photodegradation and mineralization. *Water Science and Technology* **79**, 349–355.

Zaouak, A., Noomen, A. & Jelassi, H. 2019 Gamma radiolysis of erythrosine dye in aqueous solutions. *Journal of Radioanalytical and Nuclear Chemistry* **321**, 965–971.

Zhang, L., Ding, W., Qiu, J., Jin, H., Ma, H., Li, Z. & Cang, D. 2018 Modeling and optimization study on sulfamethoxazole degradation by electrochemically activated persulfate process. *Journal of Cleaner Production* **197**, 297–305.

Zhou, T., Lu, X., Wang, J., Wong, F. & Li, Y. 2009 Rapid decolorization and mineralization of simulated textile wastewater in a heterogeneous Fenton-like system with/without external energy. *Journal of Hazardous Materials* **165**, 193–199.

Zhu, C., Jiang, C., Chen, S., Mei, R., Wang, X., Cao, J., Ma, L., Zhou, B., Wei, Q., Ouyang, G., Yu, Z. & Zhou, K. 2018 Ultrasound enhanced electrochemical oxidation of Alizarin Red S on boron-doped diamond (BDD) anode: effect of degradation process parameters. *Chemosphere* **209**, 685–695.

Zinatloo-Ajabshir, S., Morassaei, M. S. & Salavati-Niasari, M. 2019 Eco-friendly synthesis of $Nd_2Sn_2O_7$–based nanostructure materials using grape juice as green fuel as photocatalyst for the degradation of erythrosine. *Composites Part B* **167**, 643–653.

Zukawa, T., Sasaki, Y., Kurosawa, T. & Kamiko, N. 2019 Photolysis of Indigo Carmine solution by planar vacuum-ultraviolet (147 nm) light source. *Chemosphere* **214**, 123–129.

First received 29 October 2019; accepted in revised form 4 April 2020. Available online 22 April 2020

Downloaded from http://iwaponline.com/wst/article-pdf/81/5/971/768038/wst081050971.pdf
by guest